SUPPLEMENTARY MATERIALS AND METHODS

Bulk Sequencing

Bulk RNAseq was performed on fetal samples taken at GD105 (n=2), GD130 (n=2), and GD150 (n=3) (see Table S1). Tissue pieces weighing approximately 100 mg were used for RNA extraction. Total RNA was extracted from the snap-frozen tissues using TRIzol Reagent (Life Technologies, 15596-018) and a power tissue-homogenizer (OMNI-TH International, Kennesaw, GA). The RNA was purified using a Qiagen RNeasy Mini kit (Qiagen, 74104) according to the manufacturer's recommendations. An on-column DNase I digestion step was included in the purification procedure. The concentration of the eluted RNA was determined using a NanoDrop (ND-1000) spectrophotometer. Next generation sequencing of equimolar pools of cDNA libraries was performed by loading a paired-end 75bp rapid flow cell to generate a minimum of 25M raw reads on a HiSeq 2500 sequencing platform (Illumina, San Diego, CA). Raw sequencing data was submitted to Gene Expression Omnibus (GSE178680). Partek Flow was used for sequencing alignment and quantification. Ensembl IDs for rhesus were used for gene annotation. RPKM (Reads Per Kilobase of transcript, per Million mapped reads) was calculated for mRNA abundance analysis. Differentially expressed genes of rhesus lung development were identified using ANOVA with a corrected p-value (FDR) <0.05 and fold change > 1.5 between any age. Differentially expressed genes were subjected to k-means clustering, and genes with two major expression patterns (i.e., induced or suppressed with advancing gestational ages) were selected for functional enrichment analysis using ToppGene *(82)*. We compared primate data with RNA-seq data from mouse lung development time course data *(42)* (GSE122331). Genes differentially expressed during fetal lung development in mouse and rhesus macaque were directly compared.

scRNA Sequencing and Analysis

Raw sequencing data (submitted to Gene Expression Omnibus, GSE169390; also available for viewing via https://bit.ly/rhesuslung, https://bit.ly/rhesuslung_explore, https://bit.ly/rhesuslung_cellxgene) were aligned to the rhesus macaque reference Mmul_10 with Cell Ranger 3.0.2 (10x Genomics), generating expression count matrix files. Cells with fewer than 500 features or greater than 5000 features, as well as cells that contained greater than 25% of reads from mitochondrial genes, were removed. Putative multiplets were removed using *DoubletFinder (83)* (version 2.0). The *Seurat* package (version 3.1.0, https://satijalab.org/seurat/) *(41)* in R 4.0.2 was used for identification of common cell types across different experimental conditions, differential expression analysis, and most visualizations. After log-normalization, 5000 variable features were identified using the vst method for each sample, and experimental and control animal data were integrated using the *FindIntegrationAnchors* and *IntegrateData* functions with default parameters. Integrated data was scaled, and regression performed for mitochondrial genes, ribosomal genes, and cell cycle state. PCA was performed using the 5,000 most highly variable genes and the first 30 principal components (PCs), followed by *FindNeighbors()* and *FindClusters()* commands to generate UMAP clustering. Epithelial, endothelial, mesenchymal, and immune populations were identified and clustered via expression of *CDH1, PECAM1, COL1A1*, and *PTPRC* respectively, and manually annotated for further clustering. Subset objects of each cell lineage were generated for the combined control, LPS, and blockade datasets. Manual annotation of cellular identity was performed via identification of differentially expressed genes for each cluster using Seurat's implementation of the Wilcoxon rank-sum test (*FindMarkers()*) and comparing those markers to known cell type-specific genes from LungMAP *(42)*. Cell type annotations were consistent across all three treatment conditions and all objects.

These common Seurat objects were used as the basis for additional analytical tools to explore our scRNAseq data. Power analysis was performed to estimate true positive and false positive rates for populations of different cell sizes using the R package *powsimR (84)* in R 4.1.0, with default parameters. Normalized gene expression from alveolar type 2 cells from one control animal was used as input, as per package instructions, and derived parameters were used to generate 10 simulations of 2000 variable genes with 20% differentially expressed genes in the treatment condition and a nominal FDR of <0.1. We used *slingshot* v2.0 (https://github.com/kstreet13/slingshot) *(46)* and *condiments* (https://github.com/HectorRDB/condiments) *(53)* in R 4.1.0 to determine pseudotime lineage trajectories and assess differential lineages across conditions. Slingshot trajectories were generated using the *slingshot()* command with default parameters and specifying only the starting cell population. For condiments analysis, we used the *topologyTest* and *progressionTest* to estimate differential trajectories between conditions and generate p-values. PEP trajectories were identified by *Monocle3* (https://cole-trapnell-lab.github.io/monocle3/) *(85)*. For ligand-receptor analysis, we used *CellChat (56)* (https://github.com/sqjin/CellChat) v1.1 using the *SecretedSignaling* subset of the Human CellChatDB, with default parameters. Differential expression heatmaps, GO (gene ontology), pathway (PathwayCommons), and TF (GO-Elite TFTarget database) differentials were generated using *cellHarmony (86)*, using the cell-to-cluster associations from Seurat as the label file rather than alignment to the reference (--referenceType None), fold >1.2, and empirical Bayes moderated t-test <0.05 (FDR corrected). Genes with the opposite pattern of regulation in combination blockade vs. injury compared to injury vs. control, were considered restored with treatment (same statistical criterion as above). cellHarmony GO-Elite results are displayed using GraphPad Prism 9.0. Visualizations were generated by these tools, with additional use of ggplot2 when needed.

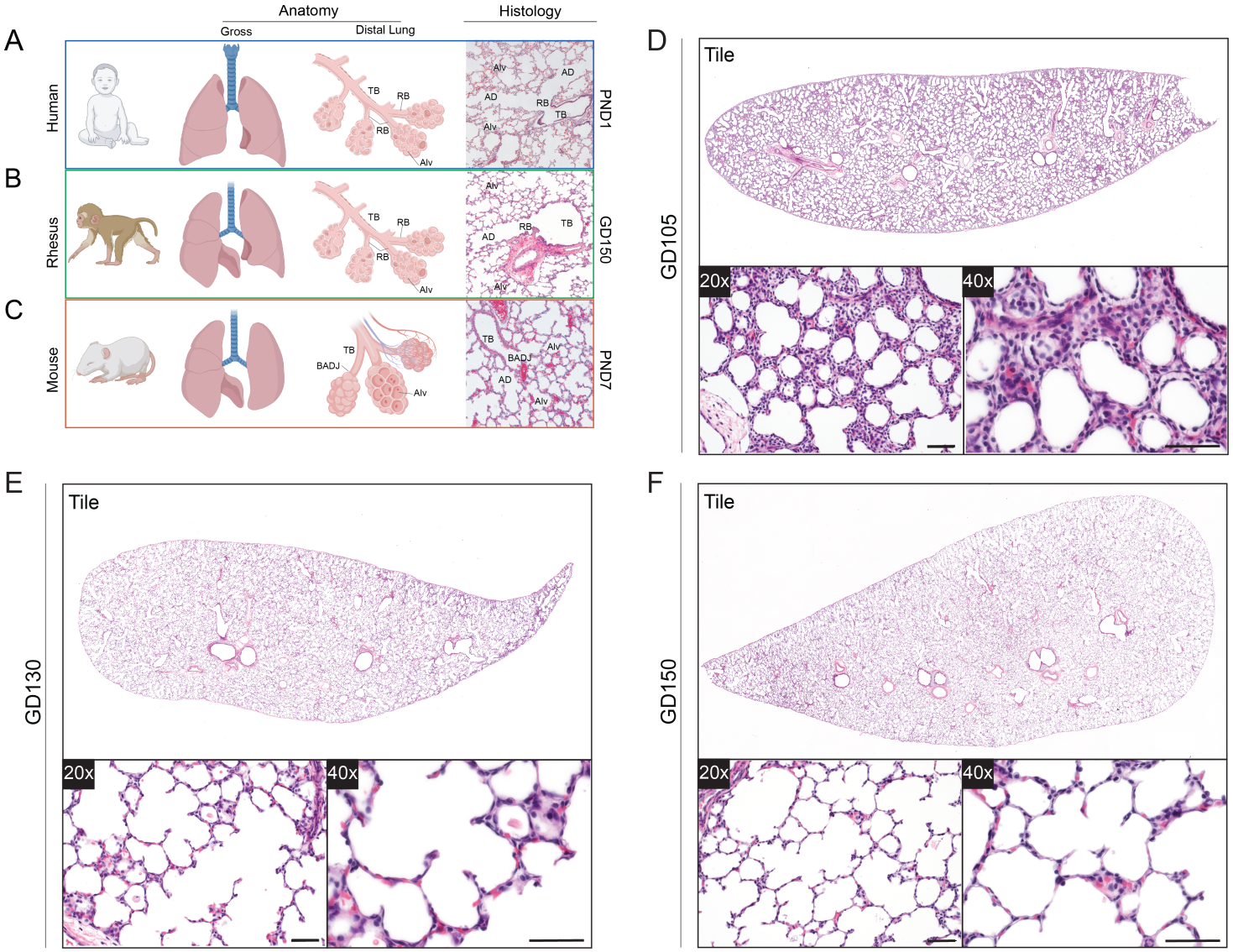

Figure S1. Rhesus macaque lung development models key aspects of human lung organogenesis. (**A** to **C**) Comparison of human, rhesus macaque, and mouse lung histologically and anatomically during the alveolar stage of development. Human lung (**A**) is organized into 3 right lobes and 2 left lobes, with a complex airway tree. The distal terminal bronchi (TB) in humans branch into respiratory bronchioles (RB), which branch into alveolar ducts (AD), that then give rise to multiple alveoli (Alv). Rhesus (**B**) are similar to human in lobar anatomy, airway complexity, and distal lung anatomy, including respiratory bronchioles, whereas murine lungs (**C**) are less branched, and terminal bronchi directly give rise to alveolar ducts at a discrete bronchoalveolar duct junction (BADJ). Alveologenesis and alveolar development occur *in utero* in humans and rhesus, whereas mice undergo alveologenesis in the first two weeks of postnatal life. (**D** to **F**) H&E of rhesus lung during the canalicular (**D**; ~GD105), saccular (**E**; ~GD130), and alveolar (**F**; ~GD150) stages of third trimester lung development show progressive alveolar maturation and gas exchange development occurs through extension of alveolar septa which are prominent by GD130 (**E**). By gestational day 150 (**F**), extensive alveolar structures are present with mature septa. Scale bars = 50 µm. *AD = Alveolar Duct; Alv = Alveolus; BADJ = Bronchoalveolar Duct Junction; GD = Gestational Day; PND = Postnatal Day; RB = Respiratory Bronchiole; TB = Terminal Bronchiole*.

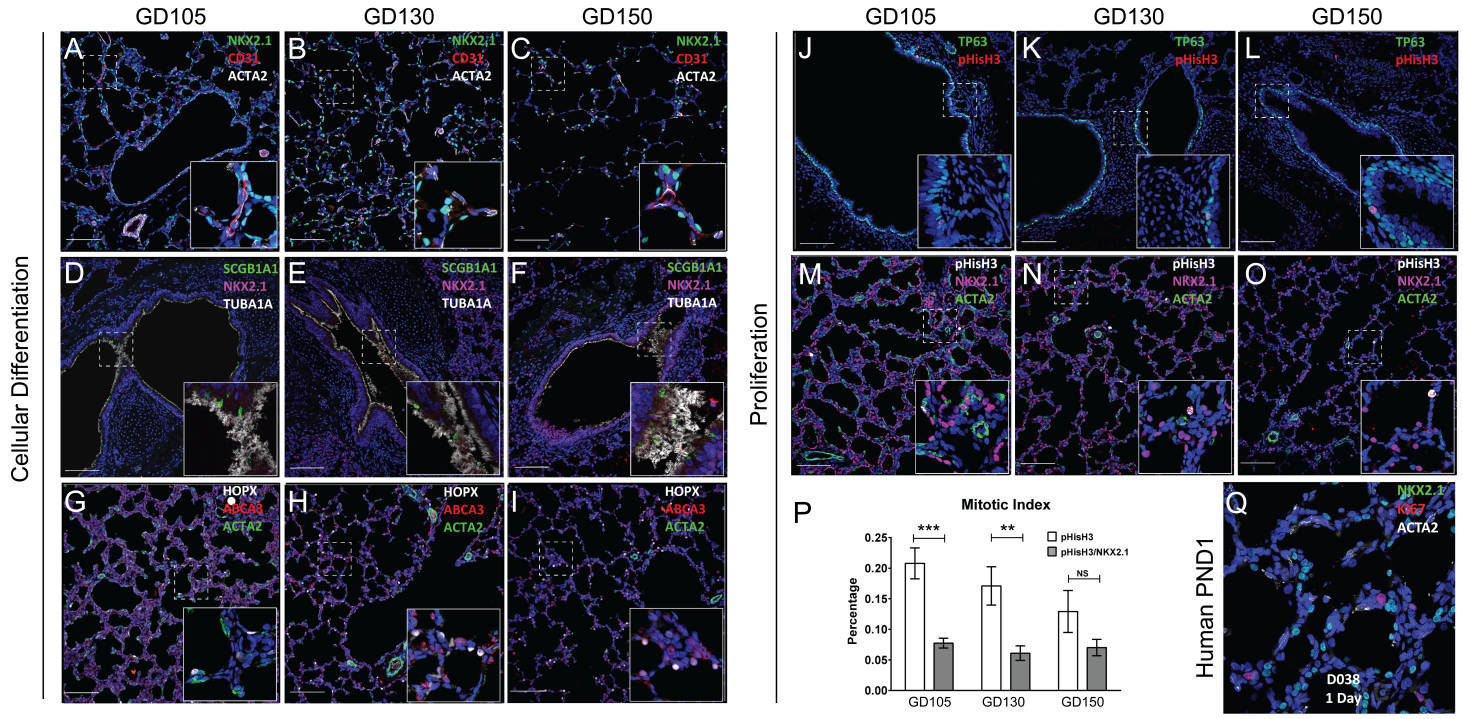

Figure S2. Progressive cellular maturation of the rhesus lung during third trimester gestation. (**A** to **I**) Confocal imaging of epithelial, mesenchymal, and endothelial lineages over the canalicular (**A, D, G**; ~GD105), saccular (**B, E, H**; ~GD130), and alveolar (**C, F, I**; ~GD150) stages of lung development. (**A** to **C**) Co-development of NKX2.1$^+$ epithelium, CD31/PECAM$^+$ endothelium, and ACTA2$^+$ myofibroblast lineages, with ultimate formation of mature capillary networks in close proximity to both epithelial and mesenchymal lineages. (**D** to **F**) Progressive differentiation of NKX2.1$^+$ epithelium with SCGB1A1$^+$ secretory cells and TUBA1A$^+$ ciliated cells to develop mature airway structures in preparation for air breathing. (**G** to **I**) Progressive differentiation and maturation of the alveolar epithelium shown through the presence of HOPX$^+$ AT1 cells and ABCA3$^+$ AT2 cells forming networks with ACTA2$^+$ mesenchymal lineages. (**J** to **P**) Examination of proliferative dynamics in the developing lung. Proliferation decreases as differentiation increases over the period of alveolarization. (**P**) Quantification obtained by counting phosphorylated Histone H3 (pHisH3) cells and comparing to DAPI$^+$ nuclei (white bars) or NKX2.1$^+$ epithelial cells (grey bars). Significantly more proliferation is seen in nonepithelial cells. (**Q**) Postnatal day 1 (PND1) human lung, showing similar maturation and morphology in the context of both NKX2.1$^+$ epithelial cells and ACTA2$^+$ mesenchymal cells when compared to GD150 rhesus fetal lung. ** = $p < 0.01$, *** = $p < 0.001$ by Student's t-test. Image inset panels are representative of regions outlined with dashed white boxes. Scale bars = 200μm.

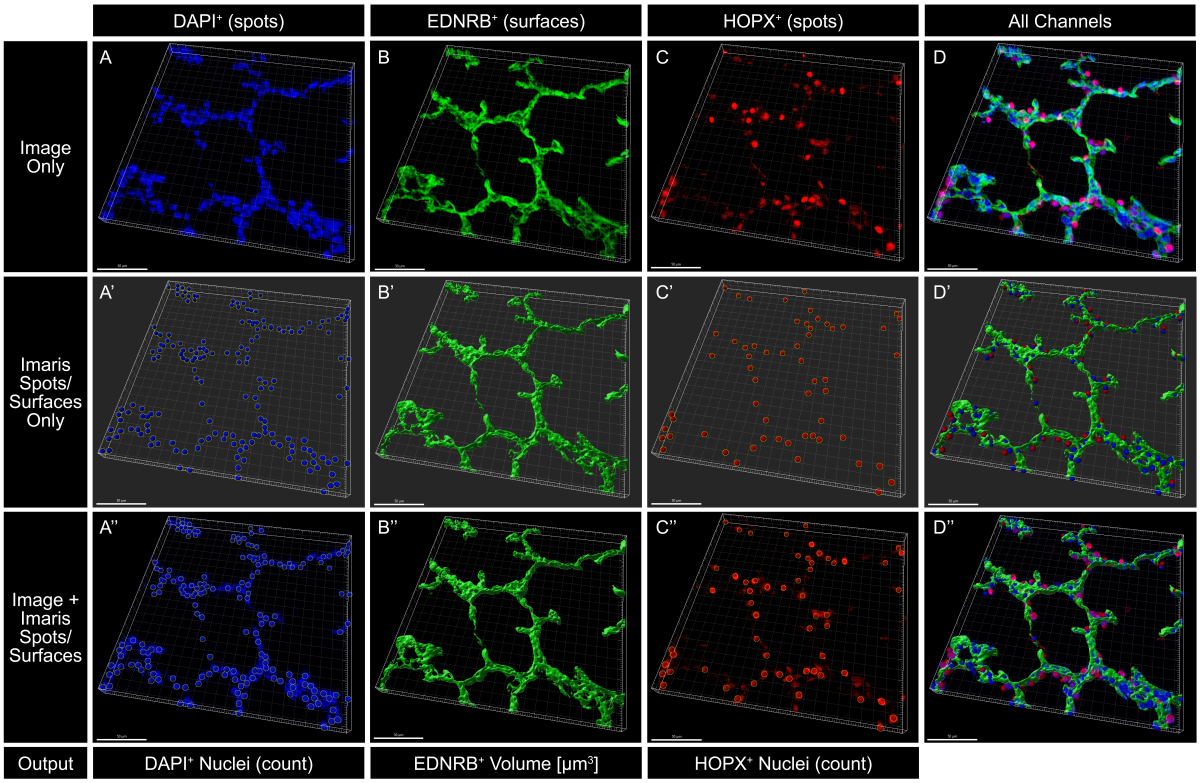

Figure S3. Method for quantification of gas exchange surface development. Confocal z-stacks were loaded into Imaris for generation of spots for DAPI$^+$ nuclei (**A** to **A″**) to identify all cells, surfaces for EDNRB$^+$ cells (**B** to **B″**) to identify gas exchange surface volume, spots for HOPX$^+$ nuclei (**C** to **C″**) to identify AT1 cells, and a composite image of all channels (**D** to **D″**). Overlay of channels in original confocal (**A** to **D**), spot/surface rendering (**A′** to **D′**), and overlap of surfaces with original (**A″** to **D″**). Automated counts of nuclei, cell surfaces, and AT1 cells were generated per image for the quantification seen in Figures 1 and 5. Scale bars = 50 μm.

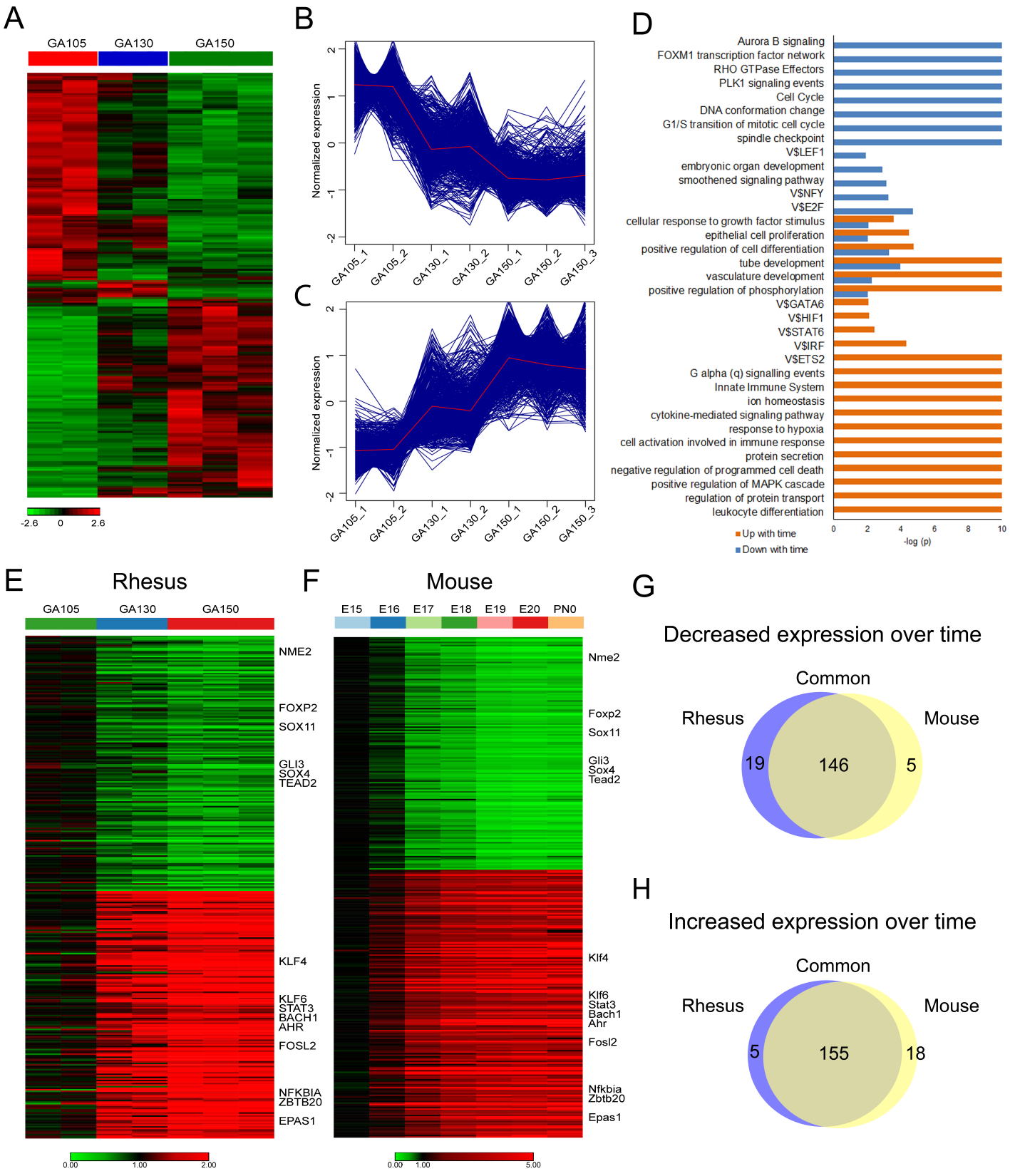

Figure S4. Bulk RNA sequencing of murine and rhesus lung during development. (**A** to **D**) Analysis of major differentially regulated genes between GD105 and GD150 in bulk lung RNAseq. Heatmap of differentially regulated genes during rhesus lung maturation (**A**) shows significant changes, with distinct gene sets decreasing (**B**) or increasing (**C**) across development. GO analysis using ToppGene *(82)* of major up (orange) and downregulated (blue) genes demonstrates progressive maturation and reduced proliferation as development proceeds. (**E** to **H**) Evaluation of major differentially regulated genes as development proceeds comparing later timepoints of rhesus to GD105 (GD105 [n=2], GD130 [n=2], GD150 [n=3] – see Table S1) (**E**) and later timepoints of mouse lung development *(42)* to E15 (**F**). Downregulated (**G**) and upregulated (**H**) genes were highly concordant between species, implying conservation of major developmental processes across mammalian evolution.

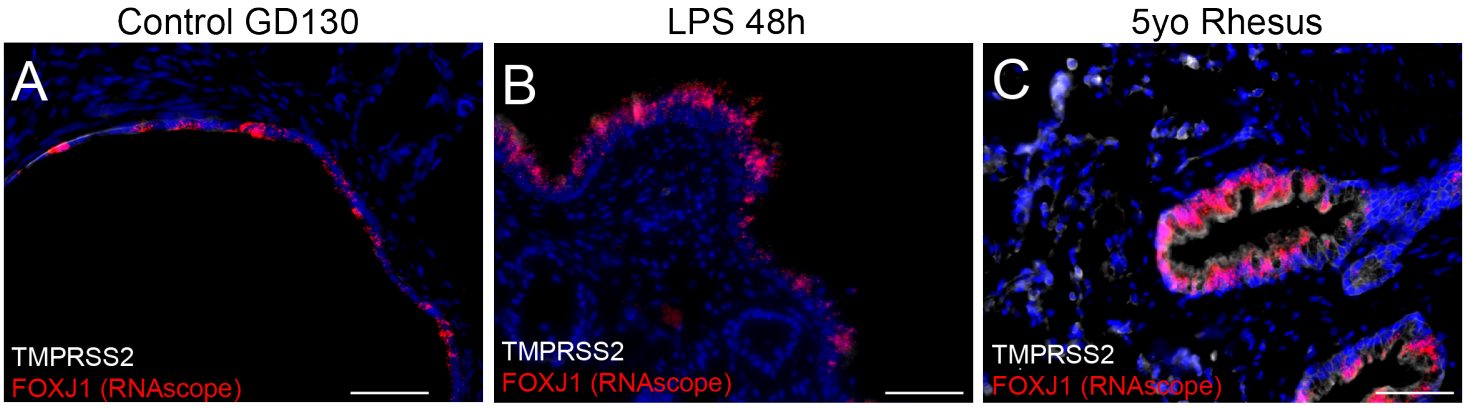

Figure S5. Low level expression of SARS-CoV-2 protease TMPRSS2 in fetal primate lung. (**A** to **C**) Evaluation of TMPRSS2 expression in fetal rhesus lung compared to adult (5yo) rhesus. Minimal expression of TMPRSS2 is evident in either the airway or alveolar regions of the developing rhesus lung (**A**) even following LPS injury (**B**). Adult rhesus lung (**C**), obtained after necropsy for non-pulmonary disease (arthritis), shows significant TMPRSS2 expression (white) in both airway and alveolar cells, also colocalizing with *FOXJ1*$^{+}$ (red) ciliated cells, concordant with age-specific expression reported in mouse and human lung *(40)*. Scale bars = 50 µm.

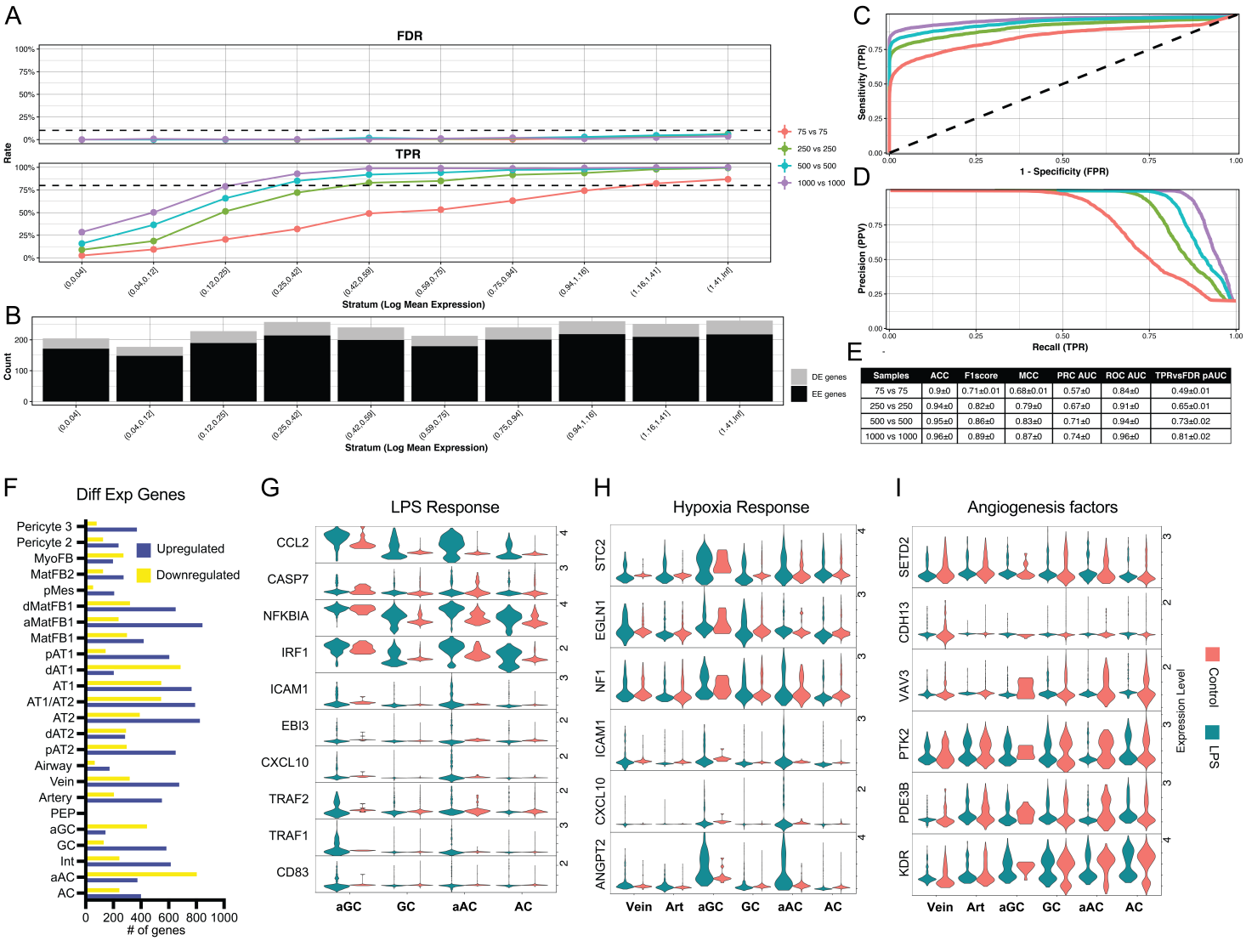

Samples	ACC	F1score	MCC	PRC AUC	ROC AUC	TPRvsFDR pAUC
75 vs 75	0.9±0	0.71±0.01	0.68±0.01	0.57±0	0.84±0	0.49±0.01
250 vs 250	0.94±0	0.82±0	0.79±0	0.67±0	0.91±0	0.65±0.01
500 vs 500	0.95±0	0.86±0	0.83±0	0.71±0	0.94±0	0.73±0.02
1000 vs 1000	0.96±0	0.89±0	0.87±0	0.74±0	0.96±0	0.81±0.02

Figure S6. Power calculations and subset analysis of scRNAseq data. (**A** to **E**) Power analysis for scRNAseq using the *powsimR* package. Power calculations done for groups of 75, 250, 500, or 1000 cells, assuming 20% differentially expressed genes between conditions and a nominal FDR of 0.1. (**A**) Conditional true positive rate (TPR) and false discovery rate (FDR) per sample size comparison per gene expression range stratum (mean ± standard error). (**B**) Number of equally (EE) and differentially expressed (DE) genes per gene expression stratum. (**C**) Receiver-Operator-Characteristics (ROC) Curve per sample size. (**D**) Precision-Recall (PR) curve per sample size tested. (**E**) Summary statistics per sample size setup rounded to two digits. (**F**) Number of differentially expressed genes that are upregulated or downregulated in each gene population with LPS compared to control. (**G** to **I**) Violin plots of gene expression for overrepresented gene categories by *cellHarmony* analysis. LPS response (**G**) and hypoxia response (**H**) are notable in multiple endothelial populations after LPS, while a subset of pro-angiogenic factors (**I**) show reduced gene expression after LPS-mediated injury. Abbreviations as defined in main text, specifically Figure 3.

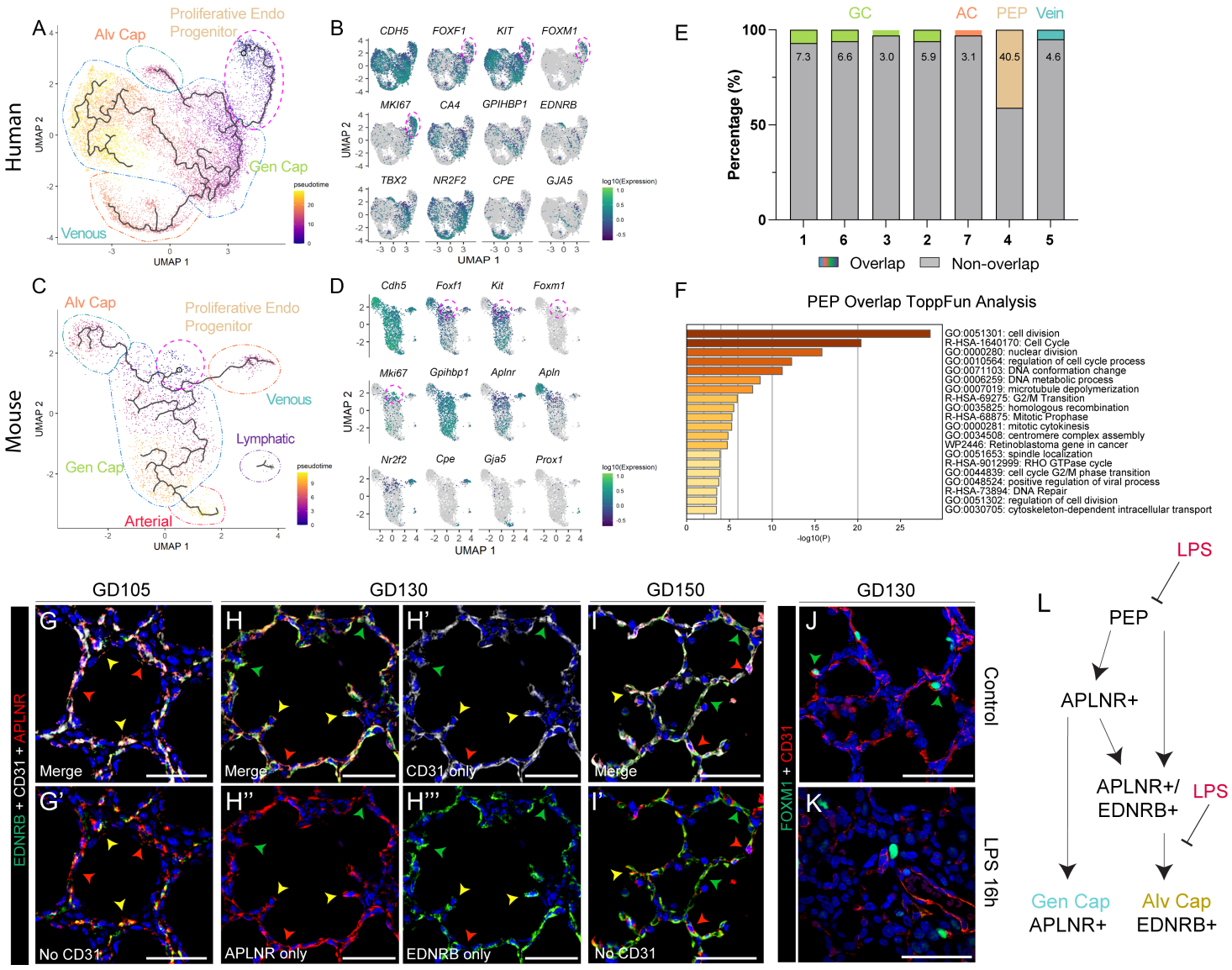

Figure S7. Conservation of the proliferative endothelial progenitor lineage across mammalian evolution. Single-cell RNA-seq (scRNAseq) analysis identifies proliferative endothelial progenitor (PEP) cells in fetal human lung and developmental mouse lung. (**A** to **B**) *Monocle3 (85)* pseudotime analysis of scRNAseq of vascular endothelial (EC) cells from fetal human lung predicted a differentiation lineage from the proliferative EC progenitor to alveolar capillaries, general capillaries, and venous like cells (data displayed originally from *(52))*. Cell identities were defined based on the expression of EC cell subtype markers including pan-EC (*CDH5)*, proliferation (*MKI67*, *FOXM1*), EC progenitor (*KIT*, *FOXF1*), general capillary (*GPIHBP1*), alveolar capillary (*TBX2*, *EDNRB)*, venous (*NR2F2*, *CPE)*, and arterial (*GJA5)* cell markers. Arterial cells make up a small portion of cells in this dataset. Proliferative EC progenitor cells co-expressed *FOXF1*, *KIT*, and *FOXM1*. (**C** to **D**) The proliferative EC progenitor is also identified in Drop-seq of EC cells from postnatal day (PND) 3 and PND7 mouse lung *(50)*; and pseudotime analysis identifies a similar differentiation lineage from the proliferative EC progenitor to alveolar capillaries, general capillaries, venous EC, and arterial EC cells, but not to lymphatic EC cells. Cell identities were defined based on the expression of EC cell subtype markers, including pan-EC (*Cdh5*), proliferation (*Mki67, Foxm1*), EC progenitor (*Kit*, *Foxf1*), general capillary (*Gpihbp1, Aplnr*), alveolar capillary (*Apln*), venous (*Nr2f2*, *Cpe*), and arterial (*Gja5)* cell markers. (**E**) Overlap of genes with FDR <0.1 from rhesus PEP with cell populations identified in human lung in (**A**). (**F**) Enriched terms in ToppGene *(82)* GO analysis of PEP genes in overlapping set from (**E**). (**G** to **I'**) Progressive differentiation of alveolar capillary endothelial cells during alveologenesis, with extensive network at GD150 (red arrowhead = APLNR$^+$ general capillary, green arrowhead = EDNRB$^+$ alveolar capillary, yellow arrowhead = APLNR$^+$/EDNRB$^+$ intermediate endothelial cell). (**J** to **K**) PEPs are lost in LPS lung injury, with few detectable FOXM1$^+$/CD31$^+$ cells. (**L**) Model of endothelial differentiation, including data from our study. LPS interferes with proper endothelial patterning via loss of PEPs and disruption of alveolar capillary differentiation. Scale bars = 50 μm.

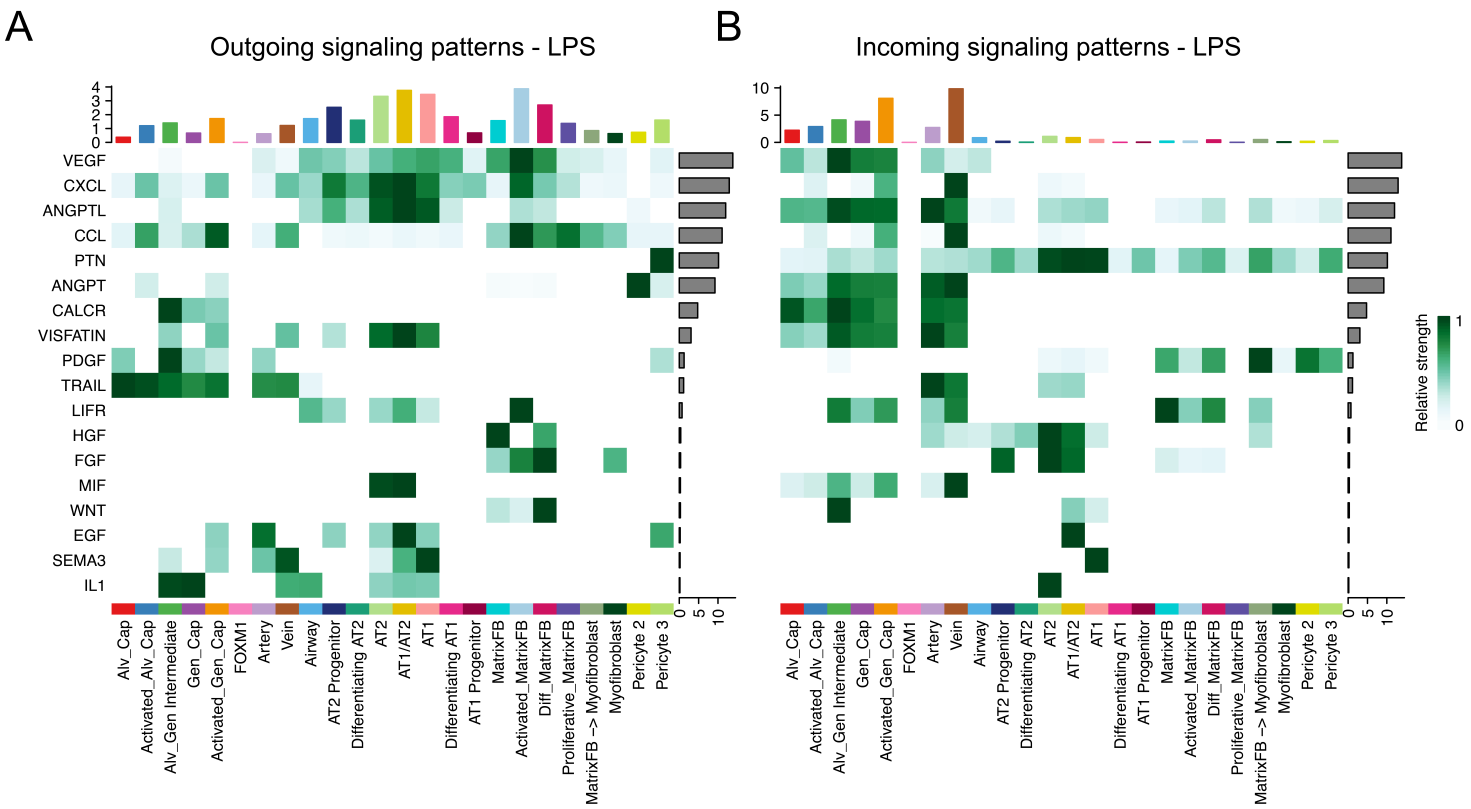

Figure S8. Major signaling patterns in LPS-treated lungs. CellChat analysis of major signaling pathways in milieu of LPS-injured primate lung. See details in Figure 4 legend. (**A**) Outgoing signaling patterns following LPS injury, with significant inflammatory pathway activation. Activated matrix fibroblasts contribute to several major inflammatory signaling pathways. (**B**) Incoming signaling pathways following LPS. CCL and CXCL responses are notable in the endothelium and epithelium.

Table S1. Rhesus Sample Information.

Animal ID	Treatment	GD	Sex	Year	H&E + Imaging	Quantification	Bulk RNAseq	scRNAseq
33-14 (LMR14-01)	Control (~GD105)	108	F	2014	✓		✓	
40-14 (LMR14-02)	Control (~GD105)	108	F	2014	✓			
41-14 (LMR14-03)	Control (~GD105)	107	M	2014	✓		✓	
24-14 (LMR14-04)	Control (~GD130)	130	M	2014	✓		✓	
28-14 (LMR14-05)	Control (~GD130)	132	F	2014	✓		✓	
44-14 (LMR14-06)	Control (~GD130)	136	F	2014	✓			
209-17	Control (~GD130)	135	F	2017	✓			
423-18	Control (~GD130)	132	M	2018	✓			
427-18	Control (~GD130)	131	M	2018	✓			
430-18	Control (~GD130)	130	M	2018	✓			
432-18	Control (~GD130)	129	M	2018	✓	✓		
506-19	Control (~GD130)	129	M	2019	✓	✓		✓
515-19	Control (~GD130)	131	F	2019	✓			✓
529-19	Control (~GD130)	130	M	2019	✓	✓		
32-14 (LMR14-07)	Control (~GD150)	152	M	2014	✓		✓	
37-14 (LMR14-08)	Control (~GD150)	151	F	2014	✓		✓	
46-14 (LMR14-10)	Control (~GD150)	144	M	2014	✓		✓	
218-17	LPS 16h	130	M	2017	✓	✓		
223-17	LPS 16h	130	F	2017	✓	✓		
429-18	LPS 16h	132	F	2018	✓			
436-18	LPS 16h	136	F	2018	✓			
437-18	LPS 16h	136	F	2018	✓			
442-18	LPS 16h	130	M	2018	✓	✓		
512-19	LPS 16h	131	F	2019	✓			✓
513-19	LPS 16h	130	F	2019	✓			✓
27-14	LPS 48h	128	F	2014	✓	✓		
36-14	LPS 48h	131	F	2014	✓	✓		
90-15	LPS 48h	127	F	2015	✓	✓		
232-17	LPS 5d	133	M	2017	✓			
233-17	LPS 5d	133	F	2017	✓	✓		
234-17	LPS 5d	133	F	2017	✓	✓		
239-17	LPS 5d	134	M	2017	✓	✓		
240-17	LPS 5d	133	M	2017	✓			
241-17	LPS 5d	133	M	2017	✓			
242-17	LPS 5d	131	F	2017	✓			
500-19	LPS + anti-TNF + IL-1RA	135	M	2019	✓	✓		
501-19	LPS + anti-TNF + IL-1RA	133	M	2019	✓			
509-19	LPS + anti-TNF + IL-1RA	135	M	2019	✓			✓
510-19	LPS + anti-TNF + IL-1RA	133	F	2019	✓	✓		✓
511-19	LPS + anti-TNF + IL-1RA	131	M	2019	✓	✓		✓
n = 40					**n = 40**	**n = 15**	**n = 7**	**n = 7**

Table S2. ImmPRESS-HRP + TSA Antibodies and Reagents.

Primary Antibody	Secondary Detection (1:100)
anti-EDNRB (mouse, R&D systems, MAB4496, 1:250) **anti-FOXM1** (rabbit, Abcam, ab207298, 1:250) **anti-Sftpc** (rabbit, Seven Hills Bioreagents, Rb458, 1:250)	**TSA Plus Fluorescein** (Akoya Biosciences, NEL741001KT)
anti-HOPX/HOP (E-1) (mouse, Santa Cruz, sc-398703, 1:500)	**TSA Plus Cyanine 3.5** (Akoya Biosciences, NEL763001KT)
anti-APLNR (rabbit, Invitrogen, 702069, 1:100) **anti-TTF1/Nkx2.1** (rabbit, Seven Hills Bioreagents, Rb1231, 1:1000)	**TSA Plus Cyanine 5** (Akoya Biosciences, NEL745001KT)

Table S3. Standard Immunofluorescence Antibodies.

Primary Antibody	Secondary Antibody (1:200)
anti-ABCA3 (guinea pig, Seven Hills Bioreagents, GP985, 1:100)	**Goat anti-Guinea Pig IgG Alexa Fluor 555** (Invitrogen, A21435)
anti-ACTA2/α-Smooth Muscle Actin (mouse IgG2a, Sigma, A5228, 1:2000)	**Donkey anti-Mouse IgG2a Alexa Fluor 633** (Invitrogen, A21136) **Donkey anti-Mouse IgG Alexa Fluor 647** (Invitrogen, A31571)
anti-HOPX/HOP (FL-73) (rabbit, Santa Cruz, SC-30216, 1:200)	**Goat anti-Rabbit IgG Alexa Fluor 488** (Invitrogen, A11034)
anti-Ki67 (mouse, BD Biosciences, 556003, 1:100)	**Goat anti-Mouse IgG1 Alexa Fluor 568** (Invitrogen, A21124)
anti-PECAM/CD31 (goat, Santa Cruz, sc-1506, 1:100)	**Donkey anti-Goat IgG Alexa Fluor 568** (Invitrogen, A11057)
anti-PECAM/CD31 (sheep, R&D Systems, AF806, 1:50)	**Donkey anti-Sheep IgG Alexa Fluor 555** (Invitrogen, A21436)
anti-pHistone H3 (Ser-10) (rabbit, Santa Cruz, sc-8656-R, 1:100)	**Goat anti-Rabbit IgG Alexa Fluor 488** (Invitrogen, A11034) **Donkey anti-Rabbit IgG Alexa Fluor 555** (Invitrogen, A31572)
anti-SCGB1A1/CCSP (rabbit, LS Biosciences, LS-B6822, 1:200)	**Goat anti-Rabbit IgG Alexa Fluor 488** (Invitrogen, A11034)
anti-TP63 (mouse, Santa Cruz, sc-71827, 1:100)	**Goat anti-Mouse IgG Alexa Fluor 488** (Invitrogen, A11001)
anti-TTF1/Nkx2.1 (guinea pig, Seven Hills Bioreagents, GP237, 1:200)	**Goat anti-Guinea Pig IgG Alexa Fluor 555** (Invitrogen, A21435)
anti-TTF1/Nkx2.1 (rabbit, Seven Hills Bioreagents, Rb1231, 1:1000)	**Goat anti-Rabbit IgG Alexa Fluor 488** (Invitrogen, A11034) **Donkey anti-Rabbit IgG Alexa Fluor 488** (Invitrogen, A21206)
anti-TUBA1A/Acetylated Tubulin (mouse IgG2b, Sigma, T7451, 1:1000)	**Donkey anti-Mouse IgG Alexa Fluor 647** (Invitrogen, A31571)

Table S4. scRNAseq Metrics.

Sample ID	506-19	515-19	512-19	513-19	509-19	510-19	511-19
Condition	**Control**	**Control**	**LPS**	**LPS**	**LPS + Blockade**	**LPS + Blockade**	**LPS + Blockade**
Estimated Number of Cells	12,458	11,797	8,710	10,502	13,935	10,785	9,465
Mean Reads per Cell	36,478	41,771	54,776	35,157	28,843	40,956	48,306
Median Genes per Cell	1,117	1,046	1,107	1,136	933	1,198	1,173
Number of Reads	4.54E+08	4.93E+08	4.77E+08	3.69E+08	4.02E+08	4.42E+08	4.57E+08
Total Genes Detected	19,630	19,568	19,506	19,382	19,595	19,735	19,461
Median UMI Counts per Cell	2,512	2,832	3,662	2,795	2,134	3,109	3,331
Valid Barcodes	96.8%	97.3%	97.8%	97.6%	96.8%	97.3%	97.0%
Sequencing Saturation	59.5%	70.5%	67.2%	56.9%	60.4%	60.1%	68.2%
Q30 Bases in Barcode	96.0%	96.6%	96.6%	96.5%	96.0%	96.6%	96.5%
Q30 Bases in RNA Read	93.8%	95.6%	95.5%	95.6%	94.1%	95.5%	95.4%
Q30 Bases in Sample Index	88.4%	95.3%	89.0%	95.8%	87.4%	92.9%	95.3%
Q30 Bases in UMI	95.8%	96.5%	96.5%	96.5%	95.8%	96.5%	96.4%
Reads Mapped to Genome	89.0%	92.9%	94.1%	94.4%	92.7%	92.7%	92.8%
Reads Mapped Confidently to Genome	84.8%	87.3%	88.1%	89.5%	87.6%	88.0%	88.0%
Reads Mapped Confidently to Intergenic Regions	21.6%	16.4%	17.1%	18.0%	17.1%	17.8%	16.5%
Reads Mapped Confidently to Intronic Regions	23.5%	24.1%	27.1%	26.8%	21.3%	22.7%	21.6%
Reads Mapped Confidently to Exonic Regions	39.7%	46.8%	43.9%	44.7%	49.2%	47.5%	50.0%
Reads Mapped Confidently to Transcriptome	37.0%	43.8%	40.8%	41.3%	45.7%	44.1%	46.6%
Reads Mapped Antisense to Gene	0.9%	0.8%	0.8%	0.9%	0.9%	0.9%	0.8%
Fraction Reads in Cells	70.6%	73.7%	90.8%	88.7%	70.3%	75.6%	69.5%